

Electron-hole pairing in graphene-GaAs heterostructures

A. Gamucci,¹ D. Spirito,¹ M. Carrega,¹ B. Karmakar,¹ A. Lombardo,² M. Bruna,²
A.C. Ferrari,² L.N. Pfeiffer,³ K.W. West,³ M. Polini,^{1,*} and V. Pellegrini^{4,1,†}

¹NEST, Istituto Nanoscienze-CNR and Scuola Normale Superiore, I-56126 Pisa, Italy

²Engineering Department, University of Cambridge, Cambridge, CB3 0FA, UK

³Department of Electrical Engineering, Princeton University, Princeton, NJ, USA

⁴Istituto Italiano di Tecnologia, Graphene labs, Via Morego 30, I-16163 Genova, Italy

Vertical heterostructures combining different layered materials offer novel opportunities for applications¹⁻³ and fundamental studies of collective behavior driven by inter-layer Coulomb coupling⁴⁻⁷. Here we report heterostructures comprising a single-layer (or bilayer) graphene carrying a fluid of massless (massive) chiral carriers⁸, and a quantum well created in GaAs 31.5 nm below the surface, supporting a high-mobility two-dimensional electron gas. These are a new class of double-layer devices composed of spatially-separated electron and hole fluids. We find that the Coulomb drag resistivity significantly increases for temperatures below 5-10 K, following a logarithmic law. This anomalous behavior is a signature of the onset of strong inter-layer correlations, compatible with the formation of a condensate of permanent excitons. The ability to induce strongly-correlated electron-hole states paves the way for the realization of coherent circuits with minimal dissipation⁹⁻¹¹ and nanodevices including analog-to-digital converters¹² and topologically protected quantum bits¹³.

Our vertical heterostructures are prepared as follows. Single-layer (SLG) and bilayer graphene (BLG) flakes are produced by micromechanical exfoliation of graphite on Si/SiO₂¹⁴. The number of layers is identified by a combination of optical microscopy¹⁵ and Raman spectroscopy^{16,17}. The latter is also used to monitor the sample quality by measuring the D to G ratio¹⁸ and the doping level¹⁹. Selected flakes are then placed onto a GaAs-based substrate at the center of a pre-patterned Hall bar by using a polymer-based wet transfer process² (see Appendix A for further details). The GaAs-based substrates consist of modulation-doped GaAs/AlGaAs heterostructures hosting a two-dimensional electron gas (2DEG) in the GaAs quantum well placed 31.5 nm below the surface. The heterostructures are grown by molecular beam epitaxy²⁰, and consist of a *n*-doped GaAs cap layer, a AlGaAs barrier, a GaAs well and a thick AlGaAs barrier with a delta doping layer (see Appendix A for further details). Two different samples are fabricated: sample A having a 15 nm-thick quantum well and sample B with a 22 nm-thick quantum well. Hall bars (300 μm wide and 1500 μm long) are fabricated by UV lithography. Ni/AuGe/Ni/Au layers are then evaporated and annealed at 400° C to form Ohmic contacts to the 2DEG, to be used for transport and Coulomb drag measurements (see Fig. 1). The Hall bar mesas are defined by conventional wet etching in acid solution. To ensure that the current in the 2DEG flows only in the region below the graphene flakes, channels with a width comparable to the transferred graphene flakes (typically $\sim 30 \mu\text{m}$), are defined in the Hall bar by means of electron beam lithography and wet etching, Figs. 1e-f). A SLG flake is transferred onto sample A and a BLG flake onto sample B. The integrity of the SLG and BLG flakes is monitored throughout the process by Raman spectroscopy. Fig. 6 in Appendix A compares the Raman spectra of as prepared SLG on Si/SiO₂ and after transfer on the GaAs substrate. Analysis of G peak position, Pos(G), its full width at half

maximum, FWHM(G), Pos(2D) and the area and intensity ratios of 2D and G peaks, allow us to monitor the amount and type of doping^{17,19,21}. This indicates a small *p* doping for the as-prepared sample, decreasing to below 100 meV for the transferred sample^{17,19,21}. The absence of a significant D peak both before and after transfer indicates that the samples have negligible amount of defects^{17,18} and that the transfer procedure does not add defects. Similarly, no increase in defects is seen for the BLG samples.

To ensure that the two-dimensional (2d) hole gas in SLG/BLG and the 2DEG in GaAs are electrically isolated, we monitor the inter-layer I_I - V_I characteristics in the 0.25 K-50 K temperature range (see Appendix C), with I_I and V_I the inter-layer (“leakage”) current and inter-layer voltage, respectively, and the layers being the SLG (or BLG) and the GaAs quantum well. In SLG-based devices, a negligible inter-layer current $< 0.2 \text{ nA}$ is measured for V_I up to -0.3 V for all temperatures, leading to inter-layer resistances $\sim 1 \text{ G}\Omega$. In the case of BLG, for $T \sim 45 \text{ K}$, I_I increases to 100 nA at $V_I = -0.3 \text{ V}$, with the inter-layer resistance increasing to several $\text{M}\Omega$. In all cases, therefore, the inter-layer resistance is much larger than the *largest* intra-layer resistance for SLG, BLG and GaAs quantum well, which is $\sim 10 \text{ k}\Omega$.

To search for signatures of correlations between the 2DEG in the GaAs quantum well and the chiral hole fluid⁸ in SLG or BLG, we measure the temperature dependence of the *Coulomb drag* resistance R_D . In a Coulomb drag experiment²²⁻²⁴ a current source is connected to one of the two layers (the *active* or *drive* layer). The other layer (the *passive* layer) is connected to an external voltmeter, so that the layer can be assumed to be an open circuit (no current can flow in it). The drive current I_{drive} drags carriers in the passive layer, which accumulate at the ends of the layer, building up an electric field. The voltage drop V_{drag} related to this field is then measured. The quantity R_D is defined as the ratio

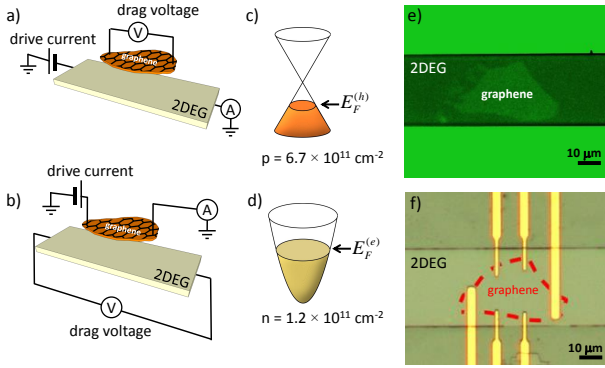


FIG. 1: Hybrid SLG/2DEG devices and Coulomb drag transport setup. a,b) Configurations for Coulomb drag measurements. In a), a voltage drop V_{drag} appears in graphene, in response to a drive current I_{drive} flowing in the 2DEG. In b) the opposite occurs. The drag voltage is measured with a low-noise voltage amplifier coupled to a voltmeter as a function of the applied bias. The drive current is also monitored. c) Conical massless Dirac fermion band structure of low-energy carriers in SLG⁸. The SLG in this work is hole doped. d) Parabolic band structure of ordinary Schrödinger electrons in the 2DEG. e) Optical micrograph of the device prior to the deposition of Ohmic contacts. The SLG flake becomes visible in green light after the sample is coated with a polymer (PMMA)¹⁵. f) Optical microscopy image of the contacted SLG on the etched 2DEG GaAs channel. The red dashed line denotes the SLG boundaries.

$V_{\text{drag}}/I_{\text{drive}}$ and is determined by the rate at which momentum is transferred between quasiparticles in the two layers²⁴.

Since R_D originates from electron-electron interactions, it contains information on many-body effects stemming from correlations^{25,26}. Experimentally, Coulomb drag has been indeed used as a sensitive probe of transitions to the superconducting state²⁷, metal-insulator transitions²⁸, transition to the Wigner crystal phase in quantum wires²⁹, and exciton condensation in quantum Hall bilayers³⁰. In the context of spatially-separated systems of electrons and holes, in the absence of a magnetic field, the theoretical studies in Ref. 31 indicated that R_D is comparable to the isolated layer resistivity in the exciton condensed phase of an electron-hole (e-h) double layer. For T larger than, but close to, the mean-field critical temperature T_c , the occurrence of e-h pairing fluctuations increases R_D with respect to its value in the Fermi-liquid phase^{32–35}. An increase in R_D with a suitable functional dependence on T indicates the transition to an exciton condensate^{32–35}. This is similar to the enhancement of conductivity in superconductors due to Cooper-pair fluctuations (“paraconductivity”) above, but close to, the critical temperature³⁶.

Prior to Coulomb drag experiments, we perform magneto-transport measurements at 4 K, as for Figs. 2a)-b). In our setup, the 2DEG is induced in the quantum well by shining light from an infrared diode. In

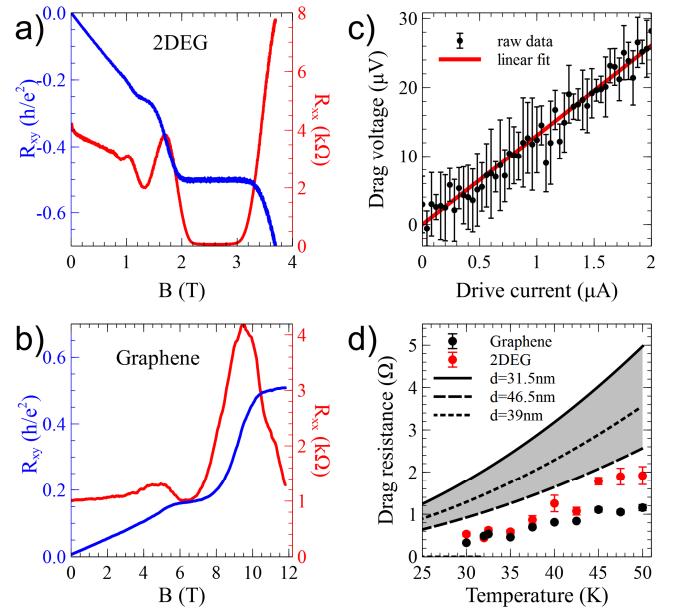


FIG. 2: Magneto-transport characterization of the 2DEG and SLG and high-temperature Coulomb drag. a,b) Hall (blue solid line) and longitudinal (red solid line) resistance of 2DEG and SLG, respectively. Hall measurements are performed in the two layers with the same configuration of electrical connections: Hall resistance is positive for holes and negative for electrons. c) Drag voltage in the 2DEG as a function of the drive current flowing in SLG at $T = 42.5$ K: data and a linear fit are shown. Error bars are calculated as standard deviations from the average of 10 current sweeps. d) Drag resistance as a function of temperature. Black (red) points refer to R_D derived by measuring the voltage drop in SLG (2DEG), respectively. The three lines are Boltzmann-transport calculations in the Fermi-liquid regime (see Ref. 40 and Appendix E). Different curves refer to different values of the inter-layer distance d : $d = 31.5$ nm (solid line), 46.5 nm (long-dashed line), and 39 nm (short-dashed line).

the SLG/2DEG device we find a 2DEG with density $n = 1.2 \times 10^{11} \text{ cm}^{-2}$ from low-field (below 1 Tesla) classical Hall effect and a mobility $\mu_e = 13000 \text{ cm}^2/(\text{Vs})$ at 4K. At $T = 45$ K, the density decreases to $4.0 \times 10^{10} \text{ cm}^{-2}$ and $\mu_e = 8700 \text{ cm}^2/(\text{Vs})$. Fig. 2a) shows the quantum Hall effect in the 2DEG. The quantum Hall plateaus at $h/(2e^2)$ and $h/(4e^2)$ (blue trace), correspond to the first two spin degenerate Landau levels³⁷. In correspondence of the plateaus, minima are found³⁷ in the longitudinal resistance R_{xx} (red trace).

The 2d hole fluids in SLG and BLG have their highest mobility when the 2DEG is *not* induced. This is shown in Fig. 2b) for the SLG-based device (see also Appendix B). Figs. 2a)-b) indicate that the sign of the Hall resistance R_{xy} in SLG is opposite to the 2DEG, thereby demonstrating that SLG is *p*-doped. At 4 K the hole density is $p = 9.9 \times 10^{11} \text{ cm}^{-2}$ and $\mu_h = 4100 \text{ cm}^2/(\text{Vs})$. At 45 K the corresponding values are $p = 6.7 \times 10^{11} \text{ cm}^{-2}$ and $\mu_h = 2400 \text{ cm}^2/(\text{Vs})$. Low-temperature magneto-transport in SLG, Fig. 2b), reveals

quantum Hall plateaus at $h/(2e^2)$ and $h/(6e^2)$, corresponding to massless Dirac fermions with spin and valley degeneracy⁸. On the contrary, when the 2DEG is optically induced, the hole density in SLG at 4 K is $p = 6.7 \times 10^{11} \text{ cm}^{-2}$ and $\mu_h = 2100 \text{ cm}^2/(\text{Vs})$, thereby weakening the manifestations of the quantum Hall effect (see Appendix B). The degradation of the SLG transport properties in the presence of the 2DEG could be linked to the creation of ionized Si donors within the n -doped GaAs cap layer, acting as positively-charged scatterers³⁸.

We now focus on the Coulomb drag experiments. These are performed in the configuration sketched in Figs. 1a)-b) and in a ³He cryostat with a 240 mK-50 K temperature range. Ten $V_{\text{drag}} - I_{\text{drive}}$ curves in a dc configuration are acquired for each T and then averaged. We first address the SLG/2DEG case. Fig. 2c) reports a representative set of averaged drag voltage data taken in the 2DEG at $T = 42.5 \text{ K}$. In this configuration, the SLG gating effect and consequent carrier depletion in the 2DEG are avoided by applying a positive current, from 0 to $+2 \mu\text{A}$ in the SLG channel. Fig. 2c) shows that at this representative value of T the drag voltage is linear with the drive current, thereby allowing the extraction of R_D from the slope of a linear fit.

Fig. 2d) plots R_D for $30 \text{ K} \leq T \leq 50 \text{ K}$, with the 2DEG used as the drive (black points) or passive (red points) layer. It also reports calculations of the T dependence of R_D in a hybrid Dirac/Schrödinger SLG/2DEG double layer within a Boltzmann-transport theory, which is justified in the Fermi-liquid regime^{39,40}. This is done by generalizing the theory of Ref. 40 to include effects due to the finite width of the GaAs quantum well (see Appendix E). This shows that the experimental results in this temperature range are consistent with the canonical Fermi-liquid prediction^{22–26,39,40}, i.e. $R_D \propto T^2$ —see also Fig. 3a)—as constrained by the available phase-space of the initial and final states involved in the scattering process. The magnitude of the measured effect, however, is smaller than predicted by theory. Discrepancies of similar magnitude have been previously reported for Coulomb drag measurements between two SLG encapsulated in hexagonal Boron Nitride⁶. Fig. 2d) demonstrates that the Onsager reciprocity relations^{41,42}, which in our case require that the resistance measured by interchanging drive and passive layers should be unchanged, are satisfied in the $30 \text{ K} \leq T \leq 40 \text{ K}$ range. A slight violation of reciprocity, whose origin is at present not understood, seems to occur for $T > 40 \text{ K}$.

We now discuss the behavior of R_D in the low- T regime. We follow Ref. 6 and use the lowest quality layer, in our case SLG, as the drive layer and measure the drag voltage in the 2DEG. In the reversed configuration, the drag voltage measured in SLG displays fluctuations^{6,7} as a function of the drive current, which hamper the extraction of R_D , see Appendix D. R_D measured in the 2DEG reveals an anomalous behavior below 10 K. Fig. 3 indicates that R_D deviates from the ordinary T^2 dependence, as shown by a large upturn for T lower than an “up-

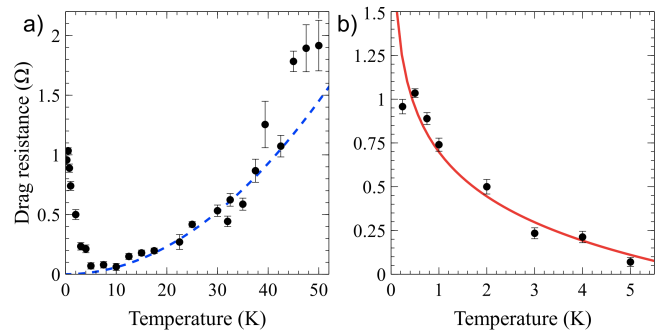


FIG. 3: Temperature dependence of the Coulomb drag resistance in the SLG/2DEG vertical heterostructure. a) R_D obtained by measuring the voltage drop in the 2DEG (passive layer) in response to a drive current flowing in the SLG (drive layer). The dashed blue line is a best-fit of the standard Fermi-liquid type²⁴: $R_D(T) = aT^2$ with $a = (5.8 \pm 0.3) \times 10^{-4} \text{ } \Omega/\text{K}^2$. b) Zoom of R_D in the low- T limit. The red solid line is a fit based on the functional form reported in Eq. (1). This fit describes very well the R_D upturn at low T as the system approaches $T_c \sim 10 \text{ mK}$ -100 mK.

turn” temperature $T_u \sim 5 \text{ K}$. The enhancement of R_D at low T is a very strong effect: the drag signal increases by more than one order of magnitude by decreasing T below T_u , where R_D is vanishingly small, in agreement with Fermi-liquid predictions (see Appendix E), down to $T = 240 \text{ mK}$.

Fig. 3b) is a zoom of the drag enhancement data in the low- T range together with a fit (solid line) of the type^{34,35}:

$$R_D(T) = R_0 + A \log \left(\frac{T_c}{T - T_c} \right), \quad (1)$$

where R_0 and A are two fitting parameters and T_c is the mean-field critical temperature of a low- T phase transition. Even though this fitting procedure cannot predict T_c , it is in excellent agreement⁴³ with the data for T_c in the range 10 mK-100 mK.

The logarithmic enhancement of R_D described by Eq. (1) was theoretically predicted in Refs. 34,35 on the basis of a Boltzmann transport theory for e-h double layers, where the scattering amplitude is evaluated in a ladder approximation³⁶. Similar results were obtained on the basis of a Kubo-formula approach³². Within these theoretical frameworks, the enhancement is attributed to e-h pairing fluctuations^{32–35,44} extending above T_c for a phase transition into an exciton condensed phase. This is ascribed to the quasi-2d nature of our SLG/2DEG heterostructure and shares similarities with other 2d systems where fluctuations play an important role like cuprate superconductors (see, for example, Ref. 45) and cold Fermi gases⁴⁶.

To further investigate this effect we explore a second device comprising of a hole-doped exfoliated BLG deposited on the surface of a GaAs quantum heterostructure. The hole density in BLG is $p = 1.4 \times 10^{12} \text{ cm}^{-2}$

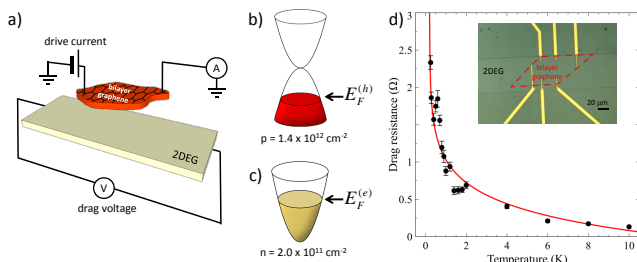


FIG. 4: **Temperature dependence of R_D in the BLG/2DEG vertical heterostructure.** a) Configuration for the Coulomb drag measurements. A voltage drop V_{drag} appears in the 2DEG in response to a current I_{drive} that flows in BLG. b) Low-energy parabolic band structure of massive chiral holes in BLG⁸. c) Parabolic band structure of Schrödinger electrons in the 2DEG. d) R_D in the low- T limit. The red solid line is a fit based on the functional form reported in Eq. (1) with $T_c \sim 190$ mK. The inset shows an optical microscopy image of the contacted BLG on the etched 2DEG GaAs channel. The red dashed line denotes the BLG boundaries.

from the low-field (below 1 Tesla) classical Hall effect and the mobility is $670 \text{ cm}^2/(\text{Vs})$ at 4 K. The 2DEG has an electron density $n = 2 \times 10^{11} \text{ cm}^{-2}$ and a mobility $86000 \text{ cm}^2/(\text{Vs})$ at 4 K. Contrary to the SLG/2DEG case, in the BLG/2DEG device both electron and hole fluids have parabolic energy-momentum dispersions, Figs. 4b)-c), recently predicted⁴⁷ to be particularly favorable for the occurrence of e-h pairing. Since e-h pairing stems from e-e interactions, a lower kinetic energy in BLG (vanishing like k^2 ²⁸ rather than like k for small values of momentum $\hbar k$) compared to SLG enhances the *relative* importance of Coulomb interactions⁴⁸ in BLG/2DEG heterostructures. To probe this, we measure the evolution of R_D as a function of T using BLG as the drive layer. Fig. 4 again shows a significant departure from the Fermi-liquid T^2 dependence. Consistent with the expected larger impact of interactions^{47,48}, we get $T_u \sim 10$ K, i.e. twice the SLG/2DEG case, while the best fit of R_D data based on Eq. (1) yields $T_c = 190$ mK (to be compared with $T_c = 10 \text{ mK}-100 \text{ mK}$ in the SLG/2DEG).

A possible approach to further increase T_u and T_c is to tune the electron n and hole p densities in the two layers in such a way to match the corresponding Fermi wave numbers, $k_F^{(e)}$ and $k_F^{(h)}$, respectively. In our devices the mismatch in the Fermi wave numbers is $\Delta k_F \equiv (k_F^{(h)} - k_F^{(e)}) / (k_F^{(h)} + k_F^{(e)}) \sim 25\%$ in the SLG/2DEG and $\Delta k_F \sim 30\%$ in the BLG/2DEG case. Such a mismatch is expected⁴⁹ to weaken the robustness of the exciton condensate phase in which condensed e-h pairs have zero total momentum $\hbar K$. Preliminary calculations⁵⁰, which include screening in the condensed phase⁵¹⁻⁵³, indicate that the $K = 0$ exciton condensate state persists even in the presence of these values of Δk_F , with T_c scales comparable to those reported here. On the other hand, a mismatch in the Fermi wave numbers of the two fluids

may favor other superfluid states, such as those discussed in Refs. 49,54-57. These states are however rather fragile in dimensionality $d > 1$, although some evidence was reported, e.g., in the layered heavy-fermion superconductor CeCoIn_5 ⁵⁸.

The topic of exciton condensation is at the front-end of current condensed-matter research and it involves experimental studies of a wide class of solid-state systems⁵⁹. Those include exciton-polaritons in semiconductor microcavities⁶⁰, which however display ultrashort (picosecond) lifetimes and optically-created indirect excitons in asymmetric semiconductor double quantum wells, where condensation competes with diffusion of the photo-created electrons and holes⁶¹. Condensation of permanent inter-layer excitons was instead demonstrated in electron-electron double layers but at the price of applying high (several Tesla) magnetic fields to enter the quantum Hall regime (see Ref. 30 and references therein). Finally, upturns of the Coulomb drag resistivity were reported in e-h doped GaAs/AlGaAs coupled quantum wells⁶²⁻⁶⁴. However, the combination of 2d electron and hole gases in the same GaAs material required a large nanofabrication effort and the reported magnitude of the drag anomalies was smaller than that found in our hybrid heterostructures. Thus our observations establish a new class of vertical heterostructure devices with a potentially large flexibility in the design of band dispersions, doping, and e-h coupling where excitonic phenomena are easily accessible.

Systems of inter-layer excitons might be used to create coherent interconnections between electronic signal processing and optical communication in integrated circuits⁹⁻¹¹ or interfaced with superconducting contacts for a variety of applications, including analog-to-digital converters¹² and topologically protected quantum bits¹³. The latter devices require, however, the exploitation of InAs-based 2DEGs that, unlike GaAs, make very good contact (i.e. no Schottky barriers) to superconductors⁶⁵. Inter-layer excitons in graphene/InAs hybrids may also pave the way for the exploration of the interplay between spin-orbit coupling and pairing fluctuations.

Acknowledgments

We thank R. Duine, R. Fazio, A. Hamilton, M. Katnelson, A. MacDonald, D. Neilson, K. Novoselov, A. Perali, A. Pinczuk, and G. Vignale for very useful discussions. We acknowledge funding from EU Graphene Flagship (contract no. CNECT-ICT-604391), EC ITN project “INDEX” Grant No. FP7-2011-289968, the Italian Ministry of Education, University, and Research (MIUR) through the program “FIRB - Futuro in Ricerca 2010” Grant No. RBFR10M5BT (“PLASMOGRAPH”), ERC grants NANOPOTS, Hetero2D, a Royal Society Wolfson Research Merit Award, EU projects GENIUS, CARERAMM, RODIN, EPSRC grants EP/K01711X/1, and EP/K017144/1.

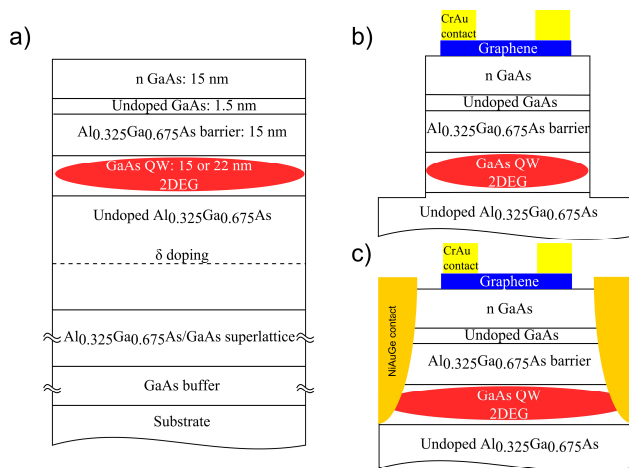


FIG. 5: a) Schematic of the GaAs/AlGaAs heterostructures (thicknesses of the layers are not to scale); b) section across the etched channel; c) section of the device along the channel.

Appendix A: Sample details and fabrication

The samples are modulation-doped GaAs/AlGaAs heterostructures hosting a 2DEG with single-layer (SLG) and bilayer graphene (BLG) flakes transferred onto them. Two different heterostructures (A and B) are investigated, differing only in the width of the quantum well, which lies 31.5 nm from the surface in both cases. The layer sequence, Fig. 5a), starting from the surface comprises a 15 nm-thick *n*-doped GaAs cap layer, followed by a 1.5 nm undoped GaAs and a 15 nm-thick undoped barrier layer of $\text{Al}_{0.325}\text{Ga}_{0.675}\text{As}$. The GaAs quantum well has a thickness of 15 nm in sample A and 22 nm in sample B; it is followed by a thick $\text{Al}_{0.325}\text{Ga}_{0.675}\text{As}$ barrier, which hosts a Si δ -doping located 48.5 nm from the well. The two samples differ in carrier density and mobility, as reported in the main text. The Hall bar devices (300 μm wide and 1.500 μm long) are fabricated by UV lithography. Ni/AuGe/Ni/Au metals are evaporated and annealed at 400° C to form Ohmic contacts to the 2DEG. The mesa is then defined by wet etching in acid solution.

SLG and BLG flakes are produced by micromechanical exfoliation¹⁴ of graphite on ~ 300 nm SiO_2 on Si substrates. The number of layers is identified by a combination of optical microscopy¹⁵ and Raman spectroscopy^{16,17}. The latter is also used to monitor the sample quality by measuring the D to G ratio¹⁸ and the doping level¹⁹. Selected flakes are then placed onto a GaAs-based substrate at the center of a pre-patterned Hall bar by using a polymer-based wet transfer process². PMMA (molecular weight 950K) is first spin coated onto the substrate with micromechanically cleaved flakes, then the sample is immersed in de-ionized water, resulting in the detachment of the polymer film because of water intercalation at the PMMA- SiO_2 interface². Graphene flakes attach to the polymer and are removed from the Si/ SiO_2

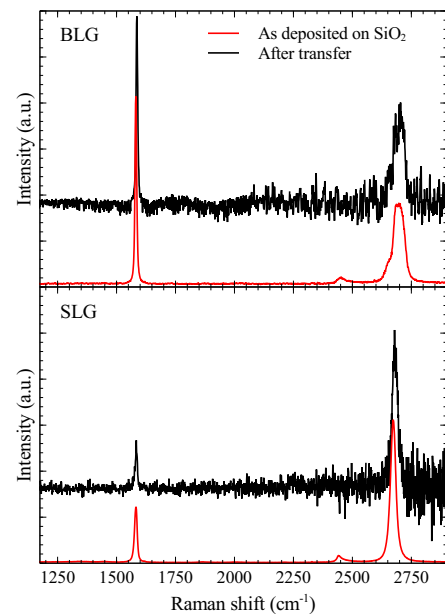


FIG. 6: Room-temperature Raman spectra of bilayer (BLG) (top panel) and single-layer (SLG) (bottom panel) graphene before and after transfer on the GaAs heterostructure.

substrate. The polymer+graphene film is then placed onto the target substrate and, after complete drying of the water, PMMA is removed by acetone. Success of the transfer is confirmed by optical inspection (bright and dark field microscopy), atomic force microscopy (AFM) and Raman spectroscopy. Raman spectra are collected with a Renishaw InVia spectrometer using laser excitation wavelengths at 514.5 nm. Excitation power is kept below 1 mW to avoid local heating and the scattered light is collected with a 100X objective. Fig. 6 plots the spectra of SLG and BLG flakes before and after transfer. The strong luminescence background due to the GaAs/AlGaAs substrate has been subtracted out in order to highlight the Raman signal of the SLG/BLG flakes after transfer. This, combined with the lack of interference enhancement on the GaAs/AlGaAs substrate, explains why the spectra of the transferred flakes are noisy. As discussed in the main text for the SLG flake, also for the BLG flake we do not see any increase of D peak, thus showing that the transfer procedure does not induce extra defects.

Since the flakes are much smaller than the Hall bar widths, in each device we define a narrow channel (~ 30 μm) in the Hall bar by electron beam lithography (EBL) and wet etching, see Figs. 5b)-c). To avoid exposure of the flakes to the electron beam, we took an optical image to align the EBL. This procedure is possible because SLG and BLG on this substrate become optically visible once coated by PMMA, see Fig. 1. Finally, Ohmic contacts (Cr/Au) are fabricated by EBL, metal evaporation and lift-off.

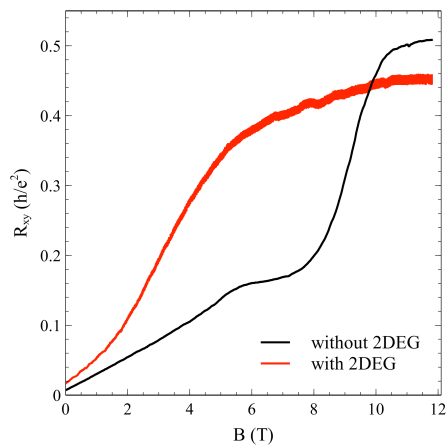


FIG. 7: Hall resistance as a function of perpendicular magnetic field in SLG at $T = 4$ K. The red curve corresponds to the case in which the 2DEG is induced by light illumination. The black curve corresponds to the case in which the GaAs quantum well is empty.

Appendix B: Electrical characterization

As described in the main text, the anomalous quantum Hall effect (QHE) in SLG is seen at 4 K when the 2DEG is *not* induced in the GaAs channel (see also black curve in Fig. 7). A markedly different result is seen when the 2DEG is induced by LED illumination. This is shown in Fig. 7, where we compare the Hall resistance at $T = 4$ K as a function of the perpendicular magnetic field up to 12 T for the two cases. Because of the massless Dirac fermion nature of the charge carriers in SLG and the spin-valley degeneracy, plateaus are expected⁶⁶ in the Hall resistance at $h/(\nu e^2)$, with $\nu = 2, 6, 10, \dots$. When the 2DEG is not induced, QHE plateaus are visible at $\nu = 2, 6$ while, as expected, the $\nu = 4$ plateau is missing. In the other case, the plateau at $\nu = 6$ is not visible and the resistance approaches the value for $\nu = 2$ at the highest magnetic field. The two configurations have different mobility, $4100 \text{ cm}^2/(\text{Vs})$, without the 2DEG, $2100 \text{ cm}^2/(\text{Vs})$ with the 2DEG. As explained in the main text, we can explain this difference considering that charged impurities (ionized Si donors) are left in the heterostructure when the 2DEG is induced, resulting in turn in an enhanced scattering of SLG carriers, which reduces mobility³⁸.

Appendix C: Inter-layer (“leakage”) current

Measurements of the leakage current between the two layers are performed by applying a voltage source to the 2DEG and detecting the current with an ammeter connected to SLG/BLG⁶⁷. The applied voltage is negative to avoid depletion of the 2DEG. We report in Fig. 8 the measured leakage currents for the SLG and BLG devices

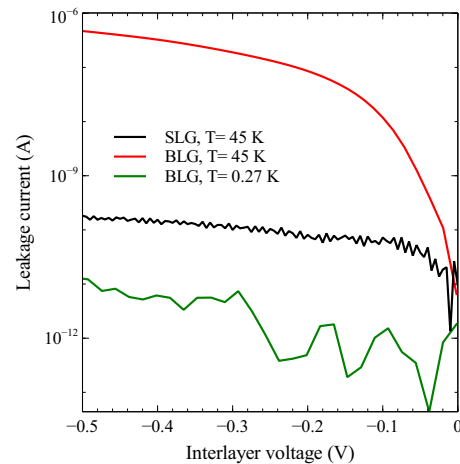


FIG. 8: Representative data for the leakage current between 2DEG and SLG/BLG as a function of the inter-layer voltage at different temperatures.

as a function of the inter-layer voltage. We recall that in the drag experiment configuration, the maximum negative value for this voltage is ~ -0.3 V. In the case of SLG, the current is smaller than 1 nA even at 45 K. In the case of BLG we find a larger current at 45 K, but still much smaller than the drive current measured in the drag experiment (in the worst case of -0.3 V we have a leakage current of ≈ 100 nA while the drive current is $2 \mu\text{A}$). At the lowest temperature, the leakage current in BLG is smaller than the drive current by many orders of magnitude, so we do not expect it to affect the drag measurement⁶.

Appendix D: Drag measured by using graphene as a passive layer

The temperature dependence of V_{drag} in SLG as a function of the drive current I_{drive} in the 2DEG is reported in Fig. 9a). Upon reducing temperature, the drag voltage measured in SLG displays a series of oscillations, which we believe to be linked to mesoscopic fluctuations already discussed in Coulomb drag setups based on two spatially-separated SLG sheets⁵⁻⁷ and also for all GaAs/AlGaAs double layers⁶⁸. These fluctuations disappear for $T \gtrsim 16$ K. Above this temperature the $V_{\text{drag}} - I_{\text{drive}}$ relation becomes linear. When the voltage drop is measured in the 2DEG no fluctuations arise at all the explored temperatures: see Fig. 9b). This allows us to extract the evolution of the drag resistance down to 250 mK (see main text). A similar fluctuating behaviour of the drag voltage at low temperature is found in sample B in the configuration in which BLG is used as the passive layer.

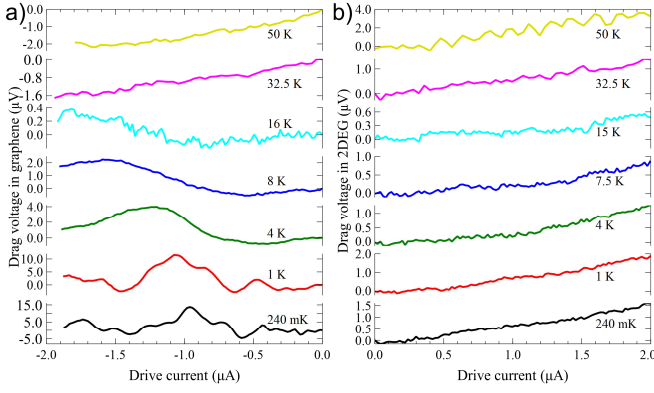


FIG. 9: Temperature dependence of the $V_{\text{drag}}-I_{\text{drive}}$ characteristics. a) The induced drag voltage measured in SLG is plotted as a function of the drive current injected in the 2DEG. b) The induced drag voltage measured in the 2DEG is plotted as a function of the drive current injected in SLG. Different traces refer to different values of the temperature, which decreases from top to bottom.

Appendix E: Theoretical background

We summarize the most elementary theory of drag resistance in the Fermi-liquid regime²⁴, which is based on Boltzmann-transport theory supplemented by second-order perturbation theory in the screened inter-layer interaction²⁴.

In the SLG/2DEG vertical heterostructure, the drag resistivity ρ_D is given, in the low-temperature limit, by⁴⁰:

$$\rho_D(T) = -\frac{1}{24e^2} \frac{1}{v_{F,t}v_{F,b}} \frac{(k_B T)^2}{\varepsilon_{F,t}\varepsilon_{F,b}} \int_0^{q_{\text{max}}} q dq |U_{tb}(q, 0)|^2 \times \mathcal{F}\left(\frac{q}{2k_{F,t}}, \frac{q}{2k_{F,b}}\right), \quad (\text{E1})$$

where $v_{F,t}$ ($v_{F,b}$) is the Fermi velocity in the top (bottom) layer, $\varepsilon_{F,t}$ ($\varepsilon_{F,b}$) is the Fermi energy in the top (bottom) layer, $k_{F,t}$ ($k_{F,b}$) is the Fermi wave number in the top (bottom) layer, $q_{\text{max}} = \min(2k_{F,t}, 2k_{F,b})$, and $\mathcal{F}(x, y) = \sqrt{(1-x^2)(1-y^2)}$. The low-temperature limit is defined by the inequality $k_B T \ll \min(\varepsilon_{F,t}, \varepsilon_{F,b})$.

In Eq. (E1) the screened interaction U_{tb} is given by:

$$U_{tb}(q, \omega) = \frac{V_{tb}(q)}{\varepsilon(q, \omega)}, \quad (\text{E2})$$

where

$$\varepsilon(q, \omega) = [1 - V_{tt}(q)\chi_t(q, \omega)][1 - V_{bb}(q)\chi_b(q, \omega)] - V_{tb}^2(q)\chi_t(q, \omega)\chi_b(q, \omega) \quad (\text{E3})$$

is the dielectric function in the random phase approximation⁴⁸. In Eq. (E3), $\chi_t(q, \omega)$ and $\chi_b(q, \omega)$ are the density-density linear response functions of the electronic fluids in the top and bottom layer, respectively. Microscopic expressions for the density-density response function $\chi_t(q, \omega)$ of the electron fluid in a doped graphene sheet can be found in Refs. 69–71. The density-density response function $\chi_b(q, \omega)$ of a 2DEG is extensively discussed in Ref. 48.

In Eqs. (E2)-(E3), $V_{tt}(q)$ is the Coulomb interaction between two charges in the top layer,

$$V_{tt}(q) = \frac{4\pi e^2 g(q)}{q(\epsilon_1 + \epsilon_2)}, \quad (\text{E4})$$

while $V_{bb}(q)$ is the Coulomb interaction in the bottom layer,

$$V_{bb}(q) = \frac{4\pi e^2 g(q)}{qD(q)} [(\epsilon_2 + \epsilon_1)e^{qd} + (\epsilon_2 - \epsilon_1)e^{-qd}], \quad (\text{E5})$$

with $D(q) = 2\epsilon_2(\epsilon_1 + \epsilon_2)e^{qd}$. Finally, the inter-layer interaction is given by

$$V_{tb}(q) = V_{bt}(q) = \frac{8\pi e^2}{qD(q)} \epsilon_2 g(q). \quad (\text{E6})$$

The dimensionless parameter ϵ_1 represents the relative dielectric constant of the material above SLG (in our case air, $\epsilon_1 = 1$), while ϵ_2 is the relative dielectric constant of GaAs, which is ~ 13 . In writing Eqs. (E4)-(E6) we neglect the difference between the dielectric constant of GaAs and AlGaAs. Note that in Eqs. (E4)-(E6) we introduced a form factor $g(q) < 1$, which stems from the finite width of the quantum well hosting the 2DEG. This can be found⁷² by solving the Poisson equation for the SLG/2DEG vertical heterostructure under the assumption that the confining potential for the 2DEG along the growth direction is given by a square quantum well of width w . This assumption has been checked with the help of a self-consistent Poisson-Schrödinger solver. We find

$$g(q) = \frac{1 - \exp(-wq)}{wq + w^3 q^3 / (4\pi^2)}. \quad (\text{E7})$$

* Electronic address: m.polini@sns.it

† Electronic address: Vittorio.Pellegrini@iit.it

¹ Novoselov, K. S. & Castro Neto, A. H. Two-dimensional crystals-based heterostructures: materials with tailored

- properties. *Phys. Scr.* **T146**, 014006 (2012).
- ² Bonaccorso, F., Lombardo, A., Hasan, T., Sun, Z., Colombo, L. & Ferrari, A. C. Production and processing of graphene and 2d crystals. *Mater. Today* **15**, 564 (2012).
 - ³ Britnell, L., Gorbachev, R. V., Jalil, R., Belle, B. D., Schedin, F., Mishchenko, A., Georgiou, T., Katsnelson, M. I., Eaves, L., Morozov, S. V., Peres, N. M. R., Leist, J., Geim, A. K., Novoselov, K. S. & Ponomarenko, L. A. Field-effect tunneling transistor based on vertical graphene heterostructures. *Science* **335**, 947-950 (2012).
 - ⁴ Ponomarenko, L. A., Geim, A. K., Zhukov, A. A., Jalil, R., Morozov, S. V., Novoselov, K. S., Grigorieva, I. V., Hill, E. H., Cheianov, V. V., Fal'ko, V. I., Watanabe, K., Taniguchi, T. & Gorbachev, R. V. Tunable metal-insulator transition in double-layer graphene heterostructures. *Nature Phys.* **7**, 958-961 (2011).
 - ⁵ Kim, S., Jo, I., Nah, J., Yao, Z., Banerjee, S. K. & Tutuc, E. Coulomb drag of massless fermions in graphene. *Phys. Rev. B* **83**, 161401(R) (2011).
 - ⁶ Gorbachev, R. V., Geim, A. K., Katsnelson, M. I., Novoselov, K. S., Tudorovskiy, T., Grigorieva, I. V., MacDonald, A. H., Morozov, S. V., Watanabe, K., Taniguchi, T. & Ponomarenko, L. A. Strong Coulomb drag and broken symmetry in double-layer graphene. *Nature Phys.* **8**, 896-901 (2012).
 - ⁷ Kim, S. & Tutuc, E. Coulomb drag and magnetotransport in graphene double layers. *Solid State Commun.* **152**, 1283 (2012).
 - ⁸ Geim, A. K. & Novoselov, K. S. The rise of graphene. *Nature Mater.* **6**, 183-191 (2007).
 - ⁹ High, A. A., Novitskaya, E. E., Butov, L. V. & Gossard, A. C. Control of exciton fluxes in an excitonic integrated circuit. *Science* **321**, 229-231 (2008).
 - ¹⁰ Kuznetsova, Y. Y., Remeika, M., High, A. A., Hammack, A. T., Butov, L. V., Hanson, M. & Gossard, A. C. All-optical excitonic transistor. *Optics Lett.* **35**, 1587-1589 (2010).
 - ¹¹ Ballarini, D., De Giorgi, M., Cancellieri, E., Houdré, R., Giacobino, E., Cingolani, R., Bramati, A., Gigli, G. & Sanvitto, D. All-optical polariton transistor. *Nature Comm.* **4**, 1778 (2013).
 - ¹² Dolcini, F., Rainis, D., Taddei, F., Polini, M., Fazio, R. & MacDonald, A. H. Blockade and counterflow supercurrent in exciton-condensate Josephson junctions. *Phys. Rev. Lett.* **104**, 027004 (2010).
 - ¹³ Peotta, S., Gibertini, M., Dolcini, F., Taddei, F., Polini, M., Ioffe, L. B., Fazio, R. & MacDonald, A. H. Josephson current in a four-terminal superconductor/exciton-condensate/superconductor system. *Phys. Rev. B* **84**, 184528 (2011).
 - ¹⁴ Novoselov, K. S., Jiang, D., Schedin, F., Booth, T. J., Khotkevich, V. V., Morozov, S. V. & Geim, A. K. *Proc. Natl. Acad. Sci. (USA)* **102**, 10451-10453 (2005).
 - ¹⁵ Casiraghi, C., Hartschuh, A., Lidorikis, E., Qian, H., Harutyunyan, H., Gokus, T., Novoselov, K. S. & Ferrari, A. C. Rayleigh imaging of graphene and graphene layers. *Nano Lett.* **7**, 2711-2717 (2007).
 - ¹⁶ Ferrari, A. C., Meyer, J. C., Scardaci, V., Casiraghi, C., Lazzeri, M., Mauri, F., Piscanec, S., Jiang, D., Novoselov, K. S., Roth, S. & Geim, A. K. Raman spectrum of graphene and graphene layers. *Phys. Rev. Lett.* **97**, 187401 (2006).
 - ¹⁷ Ferrari, A. C. & Basko, D. M. Raman spectroscopy as a versatile tool for studying the properties of graphene. *Nature Nanotech.* **8**, 235-246 (2013).
 - ¹⁸ Cancado, L. G., Jorio, A., Martins Ferreira, E. H., Stavale, F., Achete, C.A., Capaz, R. B., Moutinho, M. V. O., Lombardo, A., Kulmala, T. & Ferrari, A. C. Quantifying defects in graphene via Raman spectroscopy at different excitation energies. *Nano Lett.* **11**, 3190-3196 (2011).
 - ¹⁹ Das, A., Pisana, S., Piscanec, S., Chakraborty, B., Saha, S. K., Waghmare, U. V., Yang, R., Novoselov, K.S., Krishnamurthy, H. R., Geim, A. K., Ferrari, A. C. & Sood, A. K. Monitoring dopants by Raman scattering in an electrochemically top-gated graphene transistor. *Nature Nanotech.* **3**, 210-215 (2008).
 - ²⁰ Pfeiffer, L. N. and West, K. W. The role of MBE in recent quantum Hall effect physics discoveries. *Physica E* **20**, 57-64 (2003).
 - ²¹ Basko, D. M., Piscanec, S. & Ferrari, A. C. Electron-electron interactions and doping dependence of the two-phonon Raman intensity in graphene. *Phys. Rev. B* **80**, 165413 (2009).
 - ²² Gramila, T. J., Eisenstein, J. P., MacDonald, A. H., Pfeiffer, L. N. & West, K. W. Mutual friction between parallel two-dimensional electron systems. *Phys. Rev. Lett.* **66**, 1216-1219 (1991).
 - ²³ Sivan, U., Solomon, P. M. & Shtrikman, H. Coupled electron-hole transport. *Phys. Rev. Lett.* **68**, 1196-1199 (1992).
 - ²⁴ Rojo, A. G. Electron-drag effects in coupled electron systems. *J. Phys.: Condens. Matter* **11**, R31 (1999).
 - ²⁵ Zheng, L. & MacDonald, A. H. Coulomb drag between disordered two-dimensional electron-gas layers. *Phys. Rev. B* **48**, 8203-8209 (1993).
 - ²⁶ Kamenev, A. & Oreg, Y. Coulomb drag in normal metals and superconductors: Diagrammatic approach. *Phys. Rev. B* **52**, 7516-7527 (1995).
 - ²⁷ Giordano, N. & Monnier, J. D. Cross-talk effects in superconductor-insulator-normal-metal trilayers. *Phys. Rev. B* **50**, 9363-9368 (1994).
 - ²⁸ Pillarisetty, R., Noh, H., Tutuc, E., De Poortere, E. P., Lai, K., Tsui, D. C. & Shayegan, M. Coulomb drag near the metal-insulator transition in two dimensions. *Phys. Rev. B* **71**, 115307 (2005).
 - ²⁹ Yamamoto, M., Stopa, M., Tokura, Y., Hirayama, Y. & Tarucha, S. Negative Coulomb drag in a one-dimensional wire. *Science* **313**, 204-207 (2006).
 - ³⁰ Nandi, D., Finck, A. D. K., Eisenstein, J. P., Pfeiffer, L. N. & West, K. W. Exciton condensation and perfect Coulomb drag. *Nature* **488**, 481-484 (2012).
 - ³¹ Vignale, G. & MacDonald, A. H. Drag in paired electron-hole layers. *Phys. Rev. Lett.* **76**, 2786-2789 (1996).
 - ³² Hu, B. Y.-K. Prospecting for the superfluid transition in electron-hole coupled quantum wells using Coulomb drag. *Phys. Rev. Lett.* **85**, 820-823 (2000).
 - ³³ Snoke, D. Spontaneous Bose coherence of excitons and polaritons. *Science* **298**, 1368-1372 (2002).
 - ³⁴ Mink, M. P., Stoof, H. T. C., Duine, R. A., Polini, M. & Vignale, G. Probing the topological exciton condensate via Coulomb drag. *Phys. Rev. Lett.* **108**, 186402 (2012).
 - ³⁵ Mink, M. P., Stoof, H. T. C., Duine, R. A., Polini, M. & Vignale, G. Unified Boltzmann transport theory for the drag resistivity close to an interlayer-interaction-driven second-order phase transition. *Phys. Rev. B* **88**, 235311 (2013).
 - ³⁶ Larkin, A. & Varlamov, A. *Theory of Fluctuations in Superconductors* (Clarendon Press, Oxford, 2004).
 - ³⁷ Prange, R. E. & Girvin, S. M. *The Quantum Hall Effect*

- (Springer-Verlag, New York, 1990).
- ³⁸ Das Sarma, S., Adam, S., Hwang, E. H. & Rossi, E. Electronic transport in two-dimensional graphene. *Rev. Mod. Phys.* **83**, 407-470 (2011).
- ³⁹ Carrega, M., Tudorovskiy, T., Principi, A., Katsnelson, M. I. & Polini, M. Theory of Coulomb drag for massless Dirac fermions. *New J. Phys.* **14**, 063033 (2012).
- ⁴⁰ Principi, A., Carrega, M., Asgari, R., Pellegrini, V. & Polini, M. Plasmons and Coulomb drag in Dirac/Schrödinger hybrid electron systems. *Phys. Rev. B* **86**, 085421 (2012).
- ⁴¹ Onsager, L. Reciprocal relations in irreversible processes. I. *Phys. Rev.* **37**, 405-426 (1931).
- ⁴² Onsager, L. Reciprocal relations in irreversible processes. II. *Phys. Rev.* **38**, 2265-2279 (1931).
- ⁴³ E.g., fixing $T_c = 10$ mK, the best fit yields $A = (0.416 \pm 0.015) \Omega$ and $R_0 = (2.66 \pm 0.08) \Omega$. We can well fit the experimental data by choosing any value of T_c , as long as this is substantially lower than the lowest investigated temperature, i.e. $T = 240$ mK. As it is clear from the functional form of the fitting function in Eq. (1), in this regime a change $T_c \rightarrow T'_c$ can be reabsorbed into a change of the background resistance $R_0 \rightarrow R_0 + A \log(T'_c/T_c)$.
- ⁴⁴ Rist, S., Varlamov, A. A., MacDonald, A. H., Fazio, R. & Polini, M. Photoemission spectra of massless Dirac fermions on the verge of exciton condensation. *Phys. Rev. B* **87**, 075418 (2013).
- ⁴⁵ Zhang, W., Smallwood, C. L., Jozwiak, C., Miller, T. L., Yoshida, Y., Eisaki, H., Lee, D.-H. & Lanzara, A. Signatures of superconductivity and pseudogap formation in nonequilibrium nodal quasiparticles revealed by ultrafast angle-resolved photoemission. *Phys. Rev. B* **88**, 245132 (2013).
- ⁴⁶ Feld, M., Fröhlich, B., Vogt, E., Koschorreck, M. & Köhl, M. Observation of a pairing pseudogap in a two-dimensional Fermi gas. *Nature* **480**, 75-78 (2011).
- ⁴⁷ Perali, A., Neilson, D. & Hamilton, A. R. High-temperature superfluidity in double-bilayer graphene. *Phys. Rev. Lett.* **110**, 146803 (2013).
- ⁴⁸ Giuliani, G. F. & Vignale, G. *Quantum Theory of the Electron Liquid* (Cambridge University Press, Cambridge, 2005).
- ⁴⁹ Pieri, P., Neilson, D. & Strinati, G. C. Effects of density imbalance on the BCS-BEC crossover in semiconductor electron-hole bilayers. *Phys. Rev. B* **75**, 113301 (2007).
- ⁵⁰ Perali, A. & Neilson, D., private communication.
- ⁵¹ Sodemann, I., Pesin, D. A. & MacDonald, A. H. Interaction-enhanced coherence between two-dimensional Dirac layers. *Phys. Rev. B* **85**, 195136 (2012).
- ⁵² Lozovik, Yu. E., Ogarkov, S. L. & Sokolik, A. A. Condensation of electron-hole pairs in a two-layer graphene system: correlation effects. *Phys. Rev. B* **86**, 045429 (2012).
- ⁵³ Neilson, D., Perali, A., & Hamilton, A. R. Excitonic superfluidity and screening in electron-hole bilayer systems. [arXiv:1308.0280](https://arxiv.org/abs/1308.0280).
- ⁵⁴ Fulde, P. & Ferrell, R. A. Superconductivity in a strong spin-exchange field. *Phys. Rev.* **135**, A550-A563 (1964).
- ⁵⁵ Larkin A. J. & Ovchinnikov, Y. N. Inhomogeneous state of superconductors. *Sov. Phys. JEPT* **20**, 762 (1965).
- ⁵⁶ Casalbuoni, R. & Nardulli, G. Inhomogeneous superconductivity in condensed matter and QCD. *Rev. Mod. Phys.* **76**, 263-320 (2004).
- ⁵⁷ Subaşı, A. L., Pieri, P., Senatore, G. & Tanatar, B. Stability of Sarma phases in density imbalanced electron-hole bilayer systems. *Phys. Rev. B* **81**, 075436 (2010).
- ⁵⁸ Bianchi, A., Movshovich, R., Capan, C., Pagliuso, P. G. & Sarrao, J. L. Possible Fulde-Ferrell-Larkin-Ovchinnikov superconducting state in CeCoIn₅. *Phys. Rev. Lett.* **91**, 187004 (2003).
- ⁵⁹ For a recent review see, e.g., Rontani, M. & Sham, L. J. Coherent exciton transport in semiconductors. *Novel Superfluids Vol. 2*, edited by Bennemann, K. H. & Ketterson, J. B., International Series of Monographs on Physics no. 157 (Oxford University Press). Also available as [arXiv:1301.1726](https://arxiv.org/abs/1301.1726).
- ⁶⁰ Kasprzak, J., Richard, M., Kundermann, S., Baas, A., Jeambrun, P., Keeling, J. M. J., Marchetti, F. M., Szymańska, M. H., André, R., Staehli, J. L., Savona, V., Littlewood, P. B., Deveaud, B. & Dang, Le Si Bose-Einstein condensation of exciton polaritons. *Nature* **443**, 409-414 (2006).
- ⁶¹ High, A. A., Leonard, J. R., Hammack, A. T., Fogler, M. M., Butov, L. V., Kavokin, A. V., Campman K. L., & Gossard A. C. Spontaneous coherence in a cold exciton gas. *Nature* **483**, 584-588 (2012).
- ⁶² Croxall, A. F., Das Gupta, K., Nicoll, C. A., Thangaraj, M., Beere, H. E., Farrer, I., Ritchie, D. A. & Pepper, M. Anomalous Coulomb drag in electron-hole bilayers. *Phys. Rev. Lett.* **101**, 246801 (2008).
- ⁶³ Seamons, J. A., Morath, C. P., Reno, J. L., & Lilly, M. P. Coulomb drag in the exciton regime in electron-hole bilayers. *Phys. Rev. Lett.* **102**, 026804 (2009).
- ⁶⁴ Morath, C. P., Seamons, J. A., Reno, J. L., & Lilly, M. P. Density imbalance effect on the Coulomb drag upturn in an undoped electron-hole bilayer. *Phys. Rev. B* **79**, 041305(R) (2009).
- ⁶⁵ See, e.g., Deon, F., Pellegrini, V., Giazotto, F., Biasiol, G., Sorba, L. & Beltram, F. Quantum dot spectroscopy of proximity-induced superconductivity in a two-dimensional electron gas. *Appl. Phys. Lett.* **98**, 132101 (2011).
- ⁶⁶ Castro Neto, A. H., Guinea, F., Peres, N. M. R., Novoselov, K. S. & Geim, A. K. The electronic properties of graphene. *Rev. Mod. Phys.* **81**, 109 (2009).
- ⁶⁷ Das Gupta, L., Croxall, A. F., Waldie, J., Nicoll, C. A., Beere, H. E., Farrer, I., Ritchie, D. A. & Pepper, M. Experimental progress towards probing the ground state of an electron-hole bilayer by low-temperature transport. *Advances in Condensed Matter Physics* **2011**, 1-22 (2011).
- ⁶⁸ Price, A. S., Savchenko, A. K., Narozhny, B. N., Allison, G. & Ritchie, D. A. Giant fluctuations of Coulomb drag in a bilayer system. *Science* **316**, 99-102 (2007).
- ⁶⁹ Wunsch, B., Stauber, T., Sols, F. & Guinea, F. Dynamical polarization of graphene at finite doping. *New J. Phys.* **8**, 318 (2006).
- ⁷⁰ Hwang, E. H. & Das Sarma, S. Dielectric function, screening, and plasmons in two-dimensional graphene. *Phys. Rev. B* **75**, 205418 (2007).
- ⁷¹ Barlas, Y., Pereg-Barnea, T., Polini, M., Asgari, R. & MacDonald, A. H. Chirality and correlations in graphene. *Phys. Rev. Lett.* **98**, 236601 (2007).
- ⁷² Davies, J. *The Physics of Low-dimensional Semiconductors* (Cambridge University Press, Cambridge, 1998).